Nano Research
DOI 10.1007/s12274-014-0555-3
Research Article
ISSN 1998-0124
CN 11-5974/O4

High power triboelectric nanogenerator based on printed circuit board (PCB) technology

Changbao Han[1,§], Chi Zhang[1,§], Wei Tang[1], Xiaohui Li[1], and Zhong Lin Wang[1,2] (✉)

[1] *Beijing Institute of Nanoenergy and Nanosystems, Chinese Academy of Sciences, Beijing 100083, China*
[2] *School of Material Science and Engineering, Georgia Institute of Technology, Atlanta, Georgia 30332, USA*
[§] *These authors contributed equally to this work.*

Received: 15 July 2014
Revised: 30 July 2014
Accepted: 01 August 2014

KEYWORDS
triboelectric nanogenerator (TENG),
printed circuit board (PCB),
output power,
transformer

ABSTRACT

Harvesting mechanical energy from our surroundings to acquire a steady and high power output has attracted intensive interest due to the fast development of portable electronics. In this work, the disk-structured triboelectric nanogenerator (TENG) was prepared based on the mature printed circuit board (PCB) technology and the composite structure for effectively improving the utilization in space. A narrow grating of 1° was designed to produce high output. Operated at a rotation rate of 1,000 rpm, the TENG produces a high output power density of 267 mW/cm^2 (total power output of 25.7 W) at a matched load of 0.93 MΩ. After introducing a transformer, the output power can be managed so that it can be directly used to charge a battery for a smart phone. With the PCB production technology, fabrication of high performance TENG at low cost and large-scale becomes feasible.

1 Introduction

With improvements in microelectronics technology, portable electronics are indispensable in our daily life, which brings increasing demands on power supply [1–4]. At the same time, more and more feature-rich electronics require large increases in power consumption [5]. To meet the energy needs for portable electronics and sensor networks, harvesting mechanical energy from our surroundings is becoming a powerful approach [6–9]. Recently, the triboelectric nanogenerator (TENG) [10–12] has been demonstrated as an effective means for harvesting all kinds of mechanical energy, such as wind power [13], wave energy [14], and walking energy [15], and is likely to be a parallel technology as important as traditional generators for power generation on a large scale [16, 17]. In different kinds of TENG, the contact mode [17–19] and the sliding mode [20–22] represent the two basic types of TENGs. The sliding mode, designed with micro-sized grating structure, offers a unique and straightforward solution in harvesting energy from the relative sliding between two surfaces [23, 24]. For example, a planar-structured TENG [25], composed of radial-arrayed

Address correspondence to zlwang@gatech.edu

gratings with a central angle of 3°, generated a high output power of 1.5 W (corresponding to the power density of 19 mW/cm^2 at a rotation speed of 3,000 rpm) and theoretical calculations revealed that narrower gratings will be more effective for high output [26].

In this work, industrial printed circuit board (PCB) technology [27–29] was introduced to prepare a TENG with a composite disk structure. Two central angles of 3° and 1° for the gratings were integrated on a disk TENG to improve the space utilization and output power of the device. By means of PCB technology, TENGs can be manufactured in large quantities with high yield and lifetime. Operating at a rotation speed of 1,000 rpm, the TENG generates a short-circuit current (I_{SC}) of ~5.3 mA and an output power of 25.7 W at a matched load of ~0.93 MΩ. Through a transformer, an open-circuit voltage (V_{OC}) of 5 V and a maximum I_{SC} of 45 mA were obtained. This work not only realizes a high power output, but also paves the way for the large-scale production and application of TENGs.

2 Experimental section

Two pieces of PCB based disks were fitted coaxially. One disk is a rotor and the other is a stator. The surface of PCB based disk has a copper pattern grating embedded into the PCB base material and the detailed structure is shown in Figs. 1(a) and (b). A pair of adjacent electrodes forms the two electrodes as the output for every TENG [25]. The base materials of PCB are stiff glass epoxy for the stator and flexible polytetrafluoroethylene for the rotor. Each disk has two groups of annular-arranged copper gratings to form two TENGs—the inner TENG A and the outer TENG B. The center angles ($\Delta\theta$) of every grating or electrode for the TENG B and TENG A are 3° and 1°,

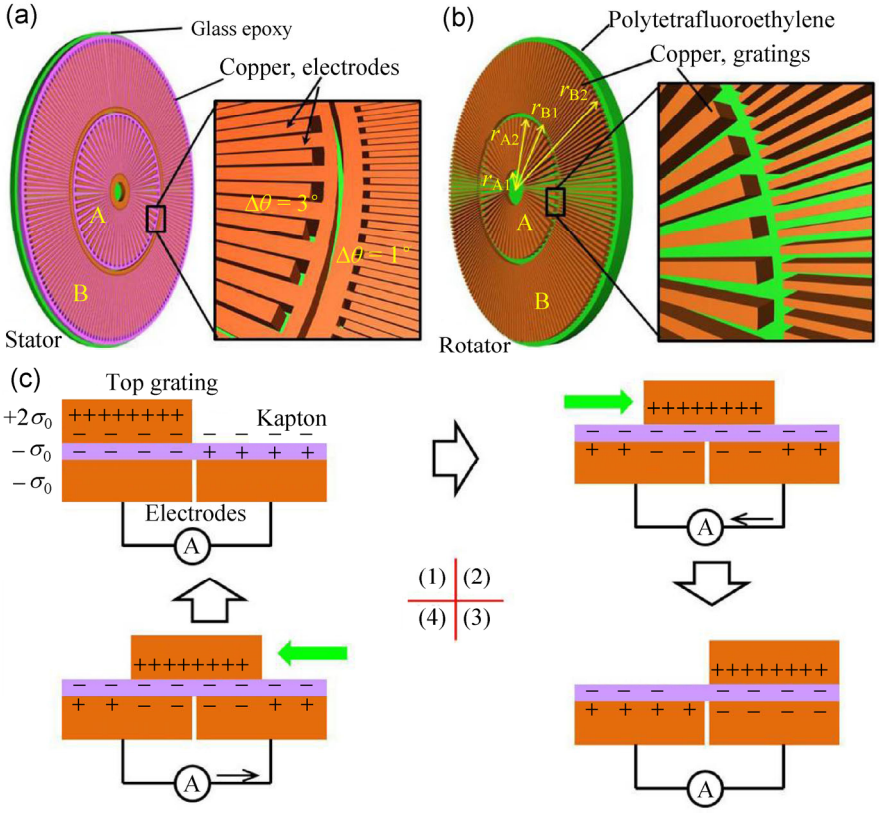

Figure 1 Schematic diagram of the TENG with a composite-disk structure: The inner TENG (a) and the outer TENG (b). The center angles of the TENG A and TENG B are 3° and 1°, respectively. (c) A sketch illustrating the electricity-generation process of the TENG in a cycle. (1) The positive triboelectric charges are generated on the top gratings and the bottom electrodes generate the inductive charges. (2) The relative motion lead to charge flow from one bottom electrode to the other because of electrostatic induction. (3) Charge flow reaches a balance at half cycle. (4) Charges flow reversely when the relative motion occurs again.

respectively. The effective radii of the two TENGs are: r_{A2} = 25 mm, r_{A1} = 6 mm, r_{B2} = 62 mm, r_{B1} = 28 mm (Fig. 1(b)). A layer of Kapton (20 μm) was treated by Ar/O_2 plasma surface treatment equipment and attached on the surface of the rotor as an electrification material to improve the triboelectrification.

The manufacturing process is accomplished using the established PCB production technology. During electrical measurement, the TENG was operated by a rotation motor. The transformer is a commercial product.

3 Result and discussion

3.1 Working principle

For the composite disk TENG, the electricity generation process is illustrated in Fig. 1(c). When the top metal grating slides along the surface of Kapton, triboelectric charges will be generated and accumulated on the surface of the two frictional materials (the top metal grating and the middle Kapton layer) [30]. Here, the charge density on the top metal gratings is twice as high as that on Kapton according to charge conservation. At the initial position, the left electrode, which is fully overlapping with a top metal grating, has negative charges and another adjacent electrode develops the same quantity of positive charges by electrostatic induction (Fig. 1(c1)). Next, after a relative sliding between the top metal grating and Kapton, the positive charges will flow from the right electrode to the left electrode and then reach another static balance (Figs. 1(c2) and 1(c3)). If the two electrodes are not shorted, there will be an electrode potential difference between the two electrodes forming an open-circuit voltage. When the top metal gratings go on sliding and become near the next electrode, the charge flow will be reversed, thereby generating a current in opposite direction. Therefore, the nanogenerator creates an alternating current (AC) output during the continuous relative rotation.

Based on previous work [25], the peak V_{OC} is determined by d and σ_0

$$V_{OC} = \frac{4d \cdot \sigma_0}{\varepsilon_0 \varepsilon_r} \quad (1)$$

where d is the thickness of Kapton, σ_0 is the triboelectric charge density on the surface of Kapton, ε_0 is the vacuum dielectric constant and ε_r is its relative dielectric constant.

For the geometry shown in Fig. 1(c), the charge density on the Kapton film is $-\sigma_0$ and is $+2\sigma_0$ on the top electrode if we ignore the edge effect. At a time t, the total amount of charge transfer between the two electrodes (Q) is

$$Q = N \cdot \sigma_0 \cdot \left(r_2^2 - r_1^2\right) \cdot \omega t \quad (2)$$

where N is the number of the gratings, ω is the angular speed (rad/s) of the disk, and r_1 and r_2 are the effective radiuses of each TENG. The detailed derivation of the formulae is presented in the Electronic Supplementary Material (ESM). So the short-circuit current (I_{SC}) is

$$I_{SC} = \frac{dQ}{dt} = \sigma_0 \cdot N \cdot \left(r_2^2 - r_1^2\right) \cdot \omega = 2\pi f N \sigma_0 \left(r_2^2 - r_1^2\right) \quad (3)$$

where f is the rotational frequency of the disk. So the frequency of the alternating electric field for the device is f'

$$f' = N \cdot f = \frac{180}{\Delta\theta} \cdot \frac{n}{60} = \frac{3n}{\Delta\theta} \quad (4)$$

where n is the rotational speed (rpm) of the disk and $\Delta\theta$ is the center angle (°) of a single electrode or metal grating (Fig. 1(a)). In this work, $\Delta\theta$ for nanogenerators A and B are 3° and 1°, respectively. Therefore, theoretically the I_{SC} is proportional to n and inversely proportional to $\Delta\theta$.

3.2 Device fabrication by PCB technology

Before preparing composite-disk TENG using PCB technology, schematic capture is a necessary step for automatic production of PCB. An electronic design automation software (Protel99se) was used and the schematic diagram is shown in Fig. S2 (in the ESM). The main subsequent steps in the manufacturing process [31] are illustrated in detail in Fig. 2 and involve: (a) Preparing the laminate: For the base material of the laminate panels, glass epoxy and flexible polytetrafluoroethylene were chosen as stator and as rotor, respectively; (b) copper coated laminate: The copper sheet covered on the laminate was prepared by cold rolling; (c) inter layer pattern transfer—dry film: Sensitive dry film; (d) inter layer pattern UV exposure

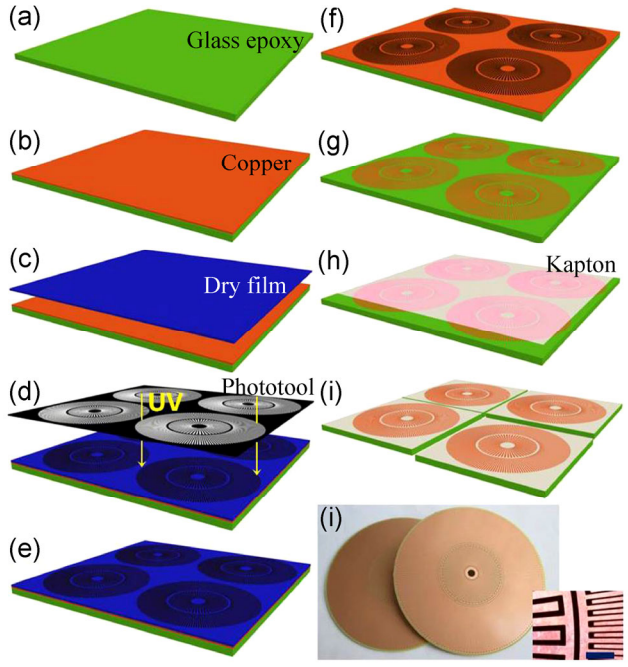

Figure 2 The large-scale preparation process of TENG based on PCB technology. (a) Preparing the laminate. (b) Copper coated laminate. (c) Inter layer pattern transferring—dry film. (d) Inter layer pattern UV exposure by phototooling. (e) Inter layer pattern developing. (f) Copper etching. (g) Inter layer strip. (h) Depositing polymer film—Kapton. (i) Cutting board. (j) Device forming. The inset of (j) is a micrograph of the device (scale, 2 mm). The process (h) is omitted during preparing the rotor.

by phototooling; (e) inter layer pattern developing: Unexposed film was wiped off to form the desired pattern by a developing solution; (f) copper etching: Using ferric chloride solution to etch away redundant copper; (g) inter layer strip: Removing the film on the copper pattern and subsequent automated optical inspection; (h) depositing the polymer film—Kapton: Attaching a layer of Kapton with high electronegativity as the tribo-layer; (i) cutting board: Cutting the whole panel with an integrated device pattern into a single device; (j) device forming. The inset of (j) is the micrograph of a fabricated device.

Using PCB technology, the narrowest gratings or intervals (between gratings) are less than 10 microns, which is beneficial for enhancing the output current. Moreover, the high yield, low cost and long life will bring the TENG closer to large-scale application.

3.3 Output performance

To test the performance of the TENG, the electrical outputs were first measured at a rotation rate of 600 rpm. For the outer nanogenerator B, the frequency f' is 1.8 Hz according to Eq. (4). As shown in Fig. 3(a), the shape of V_{OC} is similar to the superposition of triangular waves and square waves. The peak voltage of the device is about 500 V, which is similar to the theoretical analysis and previous work [25, 32]. Encouragingly, at such low rotation rate, the I_{SC} is beyond 3.5 mA, which is the first time that the continuous current supply has reached several milliamperes at this speed for a rotary TENG. The charge transfer test shows that the total quantity of transferred charge at every half cycle is 0.72 μC, similar to the integral of the current at a half cycle. The high tribo-charge density is responsible for the high output of the device. At different load resistance, the output current takes on a downswing (Fig. 3(d)). The matched load for the TENG B at a speed of 600 rpm is ~1.1 MΩ, generating an average power of 6.5 W, which corresponds to a power density of 67.6 mW/cm^2.

3.4 Tunable output and power management

As a current source, the TENG has high V_{OC} and low I_{SC} because of its high impedance compared to traditional electromagnetic nanogenerator [16]. In addition, the output current is proportional to the frequency f' of charge transport between the two electrodes according to Eqs. (3) and (4). Consequently, frequency f' changes from 0.3 to 3 kHz, corresponding to a rotation rates of 100 and 1,000 rpm, respectively, were applied to the TENG for tuning the output performance. With increase of frequency, the V_{OC} for TENG B remains fairly steady at a peak value of ~500 V (Fig. 4(a)) because the output voltage only depends on the material and device structure and is independent of the rotation rate according to Eq. (1). Then the measured current rises nearly linearly with the frequency for decreasing time in a cycle (Eq. (3)), and a 5.3 mA I_{SC} output at the rotation rate of 1,000 rpm was achieved (Fig. 4(b)). Compared with TENG B, the TENG A also has a V_{OC} of ~280 V and a maximum I_{SC} of ~0.15 mA at a rate of 1,000 rpm (Fig. S2, in the ESM). This extra output for TENG A will increase the utilization of space and this composite structure

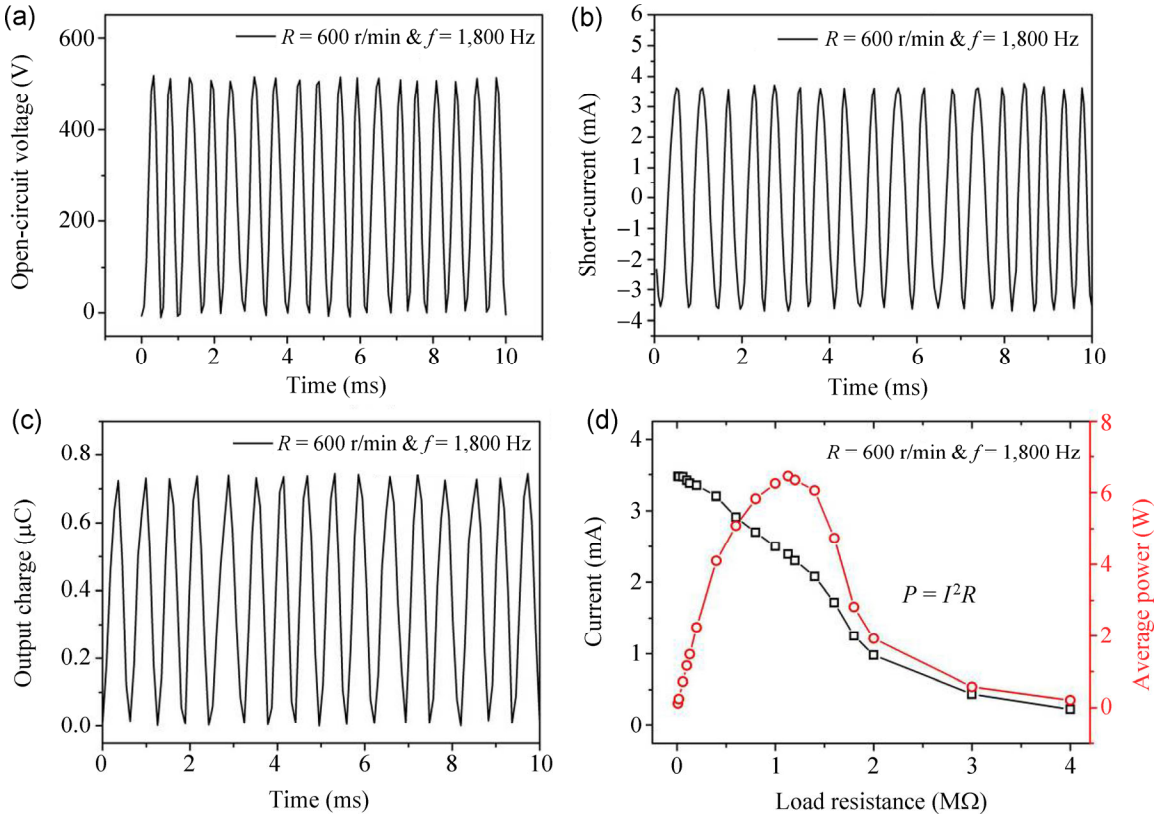

Figure 3 Measured open-circuit voltage (a), short-circuit current (b) and output charge (c) for the outer TENG at a rotation rate of 600 rpm or frequency of 1,800 Hz. (d) Output current and average power at different load resistances.

provides an efficient approach to acquire higher output per unit space for the disk TENG.

In order to acquire the maximum output power, the measured matched impedances and output powers at different frequencies are shown in Fig. 4(c). Increasing the frequency, from 600 Hz to 3 kHz, promotes an increase in the output power from 1.3 to 25.7 W (corresponding to a power density of 13.5 and 267 mW/cm^2, respectively) and brings a decrease of the matched load from 1.18 to 0.93 MΩ.

However, the large matched impedance is unfavorable for directly powering typical electronic devices. To improve the applicability, a commercial transformer was used in the output port of TENG to lower the output voltage. When the frequency is below ~2.1 KHz, with a V_{OC} of ~5 V the output current reaches 45 mA, which is 15 times that of the original output current (Figs. 4(d) and 4(e)). In the same way, as shown in Fig. 4(f), the matched load decreases with increasing frequency. Compared with the direct output of the TENG, the load is decreased by nearly three orders of magnitude, from megaohms to kiloohms, which is equivalent to the impedance of an electromagnetic generator. The reduced load can apparently be ascribed to the impedance conversion of the transformer. When the device worked at frequencies exceeding 1.8 kHz, all of the output parameters decrease quickly because of the rapid increase in losses, including copper and core losses. Via a transformer, the maximum output power for a load of 1,100 Ω and at a rotation rate of 600 rpm is ~2.2 W, which is practicable for powering typical appliances. The low conversion efficiency of the transformer probably results from the unmatched voltage, waveform or power from TENG. If the power management circuit was optimized, it should be possible to realize output powers of several hundreds of milliwatts.

3.5 Application

The mature processing technique and high output performance suggest the TENG should be applicable for electronic devices. Figure 5(a) is a photograph of a

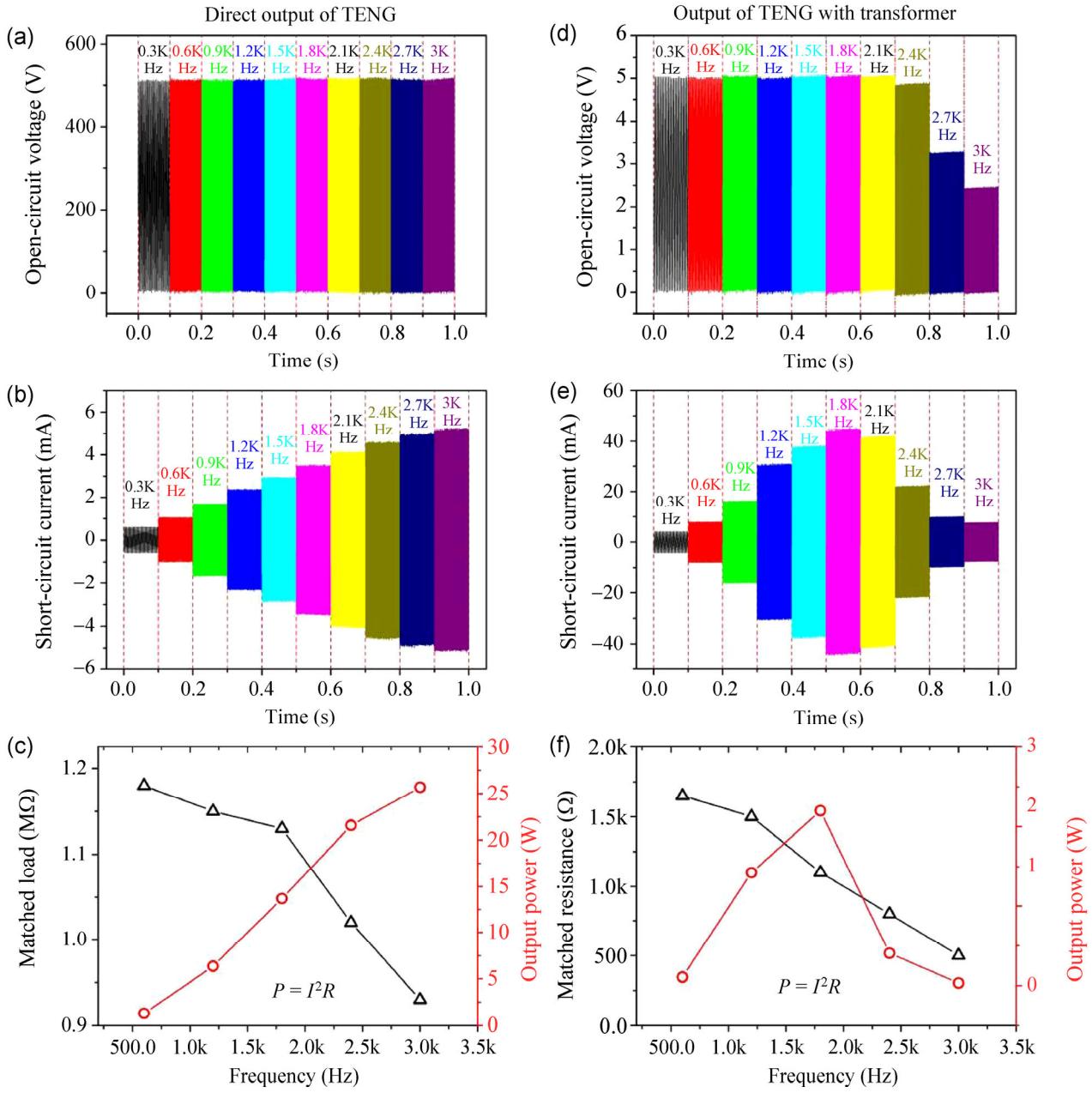

Figure 4 Output comparison of TENGs without and with power being managed by a commercial transformer. (a) and (d) Open-circuit voltage, (b) and (e) short-circuit current, and (c) and (f) load match and output power at different frequencies.

TENG based on PCB technology. When it is operated by a motor at a speed of 600 rpm, several green LEDs were lit up and the luminous intensity of a single green LED is beyond 1,000 mcd, which is equal to several candles and is sufficient to light a room. The AC signal generated directly from TENG can also power some luminescent devices, such as electroluminescent paper, and the brightness is beyond 40 cd/m^2, which is near its nominal brightness.

Harvesting mechanical energy to power potable electronics is one of our interests. Smart phones, which are indispensable in today's society, have a great need for energy. The high-power TENG makes it possible to serve as a charging source for smart phone batteries. Figure 5(e) shows a typical charging curve of a lithium ion battery (720 mAh) charged by the TENG using a transformer and a rectifier bridge. In the initial stage, it is set in a constant-current (CC)

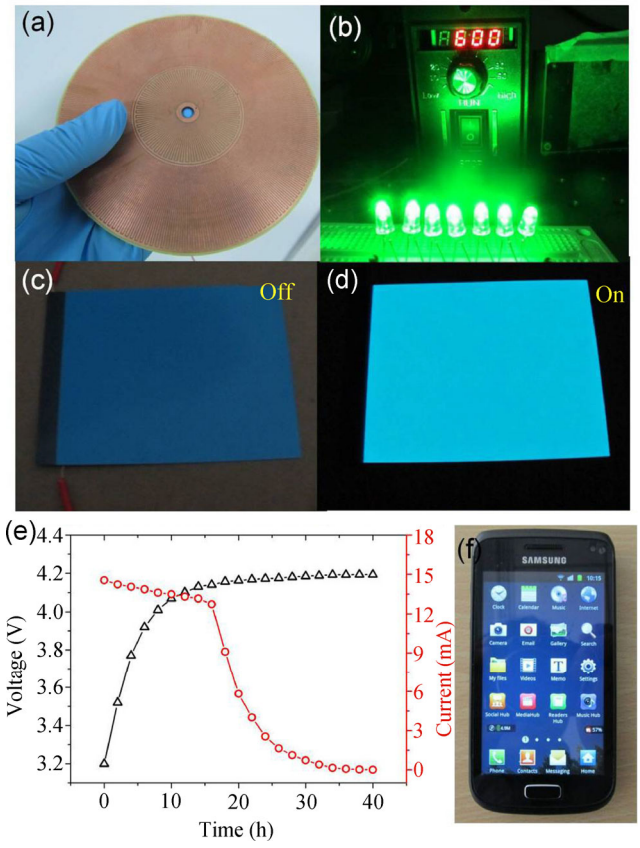

Figure 5 (a) Photograph of the TENG based on PCB. (b) Photograph of green LEDs powered by TENG at a rotation rate of 600 rpm. The luminous intensity of the single green LED is beyond 1,000 mcd. (c) and (d) Electroluminescent paper driven directly by TENG. The brightness exceeds 40 cd/m^2. (e) The voltage and current change of a lithium ion battery (720 mAh) charged by TENG after power management using a transformer. (f) Photograph of a working cell phone powered by the charged lithium ion battery.

charging mode. After about 40 h charging, the electric quantity of the battery increases from ~60% to ~95%. Figure 5(f) shows the working state of a smart phone powered by a charged lithium ion battery. The results reveal that our TENG is progressing towards use in portable electronic devices with high power. Although the charging time is still long, one must realize the volume of a cell phone battery. In case of emergency, it is very feasible to use our TENG to directly charge a cell phone so that it can make a short call.

4 Conclusion

Our work reveals that the PCB technology is a feasible and high-efficiency approach to prepare TENGs with high output power. By means of the advanced PCB technique, a composite disk-structure TENG with narrow gratings of 1° and 3° for the center angle was fabricated. When operated by a motor, the TENG produces an open-circuit voltage of ~500 V and a short-circuit current of 5.3 mA at a rotation rate of 1,000 rpm. At a matched resistance of 0.93 MΩ, a maximum output power density of 267 mW/cm^2 was reached. Via the transformer, an open-circuit voltage of 5 V and an optimal short-circuit current of 45 mA were obtained (at speed of 600 rpm), which can be directly used to charge a lithium ion battery for a cell phone. This clearly demonstrates the outstanding potential of TENG for use in portable electronics.

Acknowledgements

We are grateful for the support from the "Thousands Talents" program for Pioneer Researchers and Innovative Teams, China, and Beijing Municipal Committee of Science and Technology (Nos. Z131100006013004 and Z131100006013005). We also thank Tao Zhou and Limin Zhang for their assistance in the preparation of the device.

Electronic Supplementary Material: Supporting information (the derivation of the formulae and a schematic diagram of copper electrodes and gratings drawn by Protel99se) is available in the online version of this article at http://dx.doi.org/10.1007/s12274-014-0555-3.

References

[1] Paradiso, J. A.; Starner, T. Energy scavenging for mobile and wireless electronics. *IEEE Pervas. Comput.* **2005**, *4*, 18–27.

[2] Wang, Z. L.; Zhu, G.; Yang, Y.; Wang, S. H.; Pan, C. F. Progress in nanogenerators for portable electronics. *Mater. Today* **2012**, *15*, 532–543.

[3] Alvarado, U.; Juanicorena, A.; Adin, I.; Sedano, B.; Gutiérrez, I.; de Nó, J. Energy harvesting technologies for low-power electronics. *Trans. Emerg. Telecommun. Technol.* **2012**, *23*, 728–741.

[4] Bose, B. K. The past, present, and future of power electronics [guest introduction]. *IEEE Ind. Electron. M.* **2009**, *3*, 7–11, 14.

[5] Martinez-Garcia, S.; Dede-Garcia, E. J.; Campo-Rodriguez, J. C.; Bradley, P. J.; Rueda-Boldo, P.; Monteso-Fernandez, S.; Cagigal-Olay, C.; Vela-Garcia, R. Present and future of the power electronics (I). Introduction and high-power applications. *Dyna* **2010**, *85*, 315–330.

[6] Liu, H. C.; Zhang, S. S.; Kobayashi, T.; Chen, T.; Lee, C. Flow sensing and energy harvesting characteristics of a wind-driven piezoelectric $Pb(Zr_{0.52}, Ti_{0.48})O_3$ microcantilever. *Micro & Nano Lett.* **2014**, *9*, 286–289.

[7] Kiriakidis, G.; Kortidis, I.; Cronin, S. D.; Morris, N. J.; Cairns, D. R.; Sierros, K. A. Tribological investigation of piezoelectric ZnO films for rolling contact-based energy harvesting and sensing applications. *Thin Solid Films* **2014**, *555*, 68–75.

[8] Zhang, Z.; Liao, Q. L.; Yan, X. Q.; Wang, Z. L.; Wang, W. D.; Sun, X.; Lin, P.; Huang, Y. H.; Zhang, Y. Functional nanogenerators as vibration sensors enhanced by piezotronic effects. *Nano Res.* **2014**, *7*, 190–198.

[9] Zhang, X. H.; Fang, J. L.; Meng, F. F.; Wei, X. L. A novel self-powered wireless sensor node based on energy harvesting for mechanical vibration monitoring. *Math. Probl. Eng.* **2014**, *2014*, 642365.

[10] Fan, F. R.; Lin, L.; Zhu, G.; Wu, W. Z.; Zhang, R.; Wang, Z. L. Transparent triboelectric nanogenerators and self-powered pressure sensors based on micropatterned plastic films. *Nano Lett.* **2012**, *12*, 3109–3114.

[11] Zhu, G.; Lin, Z. H.; Jing, Q. S.; Bai, P.; Pan, C. F.; Yang, Y.; Zhou, Y. S.; Wang, Z. L. Toward large-scale energy harvesting by a nanoparticle-enhanced triboelectric nanogenerator. *Nano Lett.* **2013**, *13*, 847–853.

[12] Han, C. B.; Du, W. M.; Zhang, C.; Tang, W.; Zhang, L. M.; Wang, Z. L. Harvesting energy from automobile brake in contact and non-contact mode by conjunction of triboelectrication and electrostatic-induction processes. *Nano Energy* **2014**, *6*, 59–65.

[13] Xie, Y. N.; Wang, S. H.; Lin, L.; Jing, Q. S.; Lin, Z. H.; Niu, S. M.; Wu, Z. Y.; Wang, Z. L. Rotary triboelectric nanogenerator based on a hybridized mechanism for harvesting wind energy. *ACS Nano* **2013**, *7*, 7119–7125.

[14] Hu, Y. F.; Yang, J.; Jing, Q. S.; Niu, S. M.; Wu, W. Z.; Wang, Z. L. Triboelectric nanogenerator built on suspended 3D spiral structure as vibration and positioning sensor and wave energy harvester. *ACS Nano* **2013**, *7*, 10424–10432.

[15] Hou, T. C.; Yang, Y.; Zhang, H. L.; Chen, J.; Chen, L. J.; Wang, Z. L. Triboelectric nanogenerator built inside shoe insole for harvesting walking energy. *Nano Energy* **2013**, *2*, 856–862.

[16] Zhang, C.; Tang, W.; Han, C. B.; Fan, F. R.; Wang, Z. L. Theoretical comparison, equivalent transformation, and conjunction operations of electromagnetic induction generator and triboelectric nanogenerator for harvesting mechanical energy. *Adv. Mater.* **2014**, *26*, 3580–3591.

[17] Fan, F. R.; Tang, W.; Yao, Y.; Luo, J. J.; Zhang, C.; Wang, Z. L. Complementary power output characteristics of electromagnetic generators and triboelectric generators. *Nanotechnology* **2014**, *25*, 135402.

[18] Wang, S. H.; Lin, L.; Wang, Z. L. Nanoscale triboelectric-effect-enabled energy conversion for sustainably powering portable electronics. *Nano Lett.* **2012**, *12*, 6339–6346.

[19] Zhu, G.; Lin, Z. H.; Jing, Q. S.; Bai, P.; Pan, C. F.; Yang, Y.; Zhou, Y. S.; Wang, Z. L. Toward large-scale energy harvesting by a nanoparticle-enhanced triboelectric nanogenerator. *Nano Lett.* **2013**, *13*, 847–853.

[20] Wang, S. H.; Lin, L.; Xie, Y. N.; Jing, Q. S.; Niu, S. M.; Wang, Z. L. Sliding-triboelectric nanogenerators based on in-plane charge-separation mechanism. *Nano Lett.* **2013**, *13*, 2226–2233.

[21] Yang, Y.; Zhang, H. L.; Chen, J.; Jing, Q. S.; Zhou, Y. S.; Wen, X. N.; Wang, Z. L. Single-electrode-based sliding triboelectric nanogenerator for self-powered displacement vector sensor system. *ACS Nano* **2013**, *7*, 7342–7351.

[22] Zhang, C.; Zhou, T.; Tang, W.; Han, C. B.; Zhang, L. M.; Wang, Z. L. Rotating-disk-based direct-current triboelectric nanogenerator. *Adv. Energy Mater.* **2014**, *4*, 1301798.

[23] Zhu, G.; Zhou, Y. S.; Bai, P.; Meng, X. S.; Jing, Q. S.; Chen, J.; Wang, Z. L. A shape-adaptive thin-film-based approach for 50% high-efficiency energy generation through micro-grating sliding electrification. *Adv. Mater.* **2014**, *26*, 3788–3796.

[24] Jing, Q. S.; Zhu, G.; Bai, P.; Xie, Y. N.; Chen, J.; Han, R. P. S.; Wang, Z. L. Case-encapsulated triboelectric nanogenerator for harvesting energy from reciprocating sliding motion. *ACS Nano* **2014**, *8*, 3836–3842.

[25] Zhu, G.; Chen, J.; Zhang, T. J.; Jing, Q. S.; Wang, Z. L. Radial-arrayed rotary electrification for high performance triboelectric generator. *Nat. Commun.* **2014**, *5*, 3426.

[26] Niu, S. M.; Liu, Y.; Wang, S. H.; Lin, L.; Zhou, Y. S.; Hu, Y. F.; Wang, Z. L. Theory of sliding-mode triboelectric nanogenerators. *Adv. Mater.* **2013**, *25*, 6184–6193.

[27] Ji, P.; Wan, Y. F. Planning for printed circuit board assembly: The state-of-the-art review. *Int. J. Comput. Appl. Technol.* **2001**, *14*, 136–144.

[28] LaDou, J. Printed circuit board industry. *Int. J. Hyg. Environ. Health* **2006**, *209*, 211–219.

[29] Bonner, R. F.; Asselta, J. A.; Haining, F. W. Advanced printed-circuit board design for high-performance computer-applications. *IBM J. Res. Dev.* **1982**, *26*, 297–305.

[30] Wang, S. H.; Xie, Y. N.; Niu, S. M.; Lin, L.; Wang, Z. L. Freestanding triboelectric-layer-based nanogenerators for harvesting energy from a moving object or human motion in contact and non-contact modes. *Adv. Mater.* **2014**, *26*, 2818–2824.

[31] Bains, N.; Geraghty, K.; Goosey, M. New technologies for a sustainable printed circuit board manufacturing process. *Circuit World* **2006**, *32*, 19–24.

[32] Lin, L.; Wang, S. H.; Xie, Y. N.; Jing, Q. S.; Niu, S. M.; Hu, Y. F.; Wang, Z. L. Segmentally structured disk triboelectric nanogenerator for harvesting rotational mechanical energy. *Nano Lett.* **2013**, *13*, 2916–2923.